Published in Materials Research Bulletin (2006), Accepted Post-print (Author Version)

Enhancement of the magnetic properties of Ni–Cu–Zn ferrites with the substitution of a small fraction of lanthanum for iron

P.K. Roy and J. Bera

Department of Ceramic Engineering, National Institute of Technology 769008, India

Received 1 December 2005; revised 11 May 2006; accepted 15 May 2006. Available online 9 June 2006.

Abstract

The effect of lanthanum ion substitution for iron on the structural and magnetic properties of Ni–Cu–Zn ferrite is reported. The $(Ni_{0.25}Cu_{0.20}Zn_{0.55})La_xFe_{2-x}O_4$ ferrite compositions with x = 0.0, 0.025, 0.050 and 0.075, were synthesized by nitrate–citrate auto-combustion route. Rietveld structure refinement was carried out to evaluate; La solubility in spinel, residual stress in sintered core, quantity of secondary $LaFeO_3$ phase formed and change in lattice parameters, etc. Density, crystallite size, grain size, residual macrostress and initial permeability were directly affected by the substitution. A significant increase in initial permeability was achieved by a small fraction of La substitution. The La solubility in the Ni–Cu–Zn ferrite lattice was found very low ($\sim$0.1 atom/unit cell). Co-relations between magnetic properties and measured physical/structural properties were discussed.

Keywords: A. Ceramics; A. Magnetic materials; C. X-ray diffraction; D. Magnetic properties; D. Microstructure

1. Introduction

Ni–Cu–Zn ferrites are well established magnetic materials for multilayer chip inductor (MLCI) applications, because of their relatively low sintering temperature, high permeability in the RF frequency region and high electrical resistivity [1], [2] and [3]. For multilayer device application, the ferrite needs to be sintered at <950 °C in order to bond with the internal silver electrode during the manufacturing of MLCIs. To decrease the sintering temperature, fine ferrite powder (small grain size and reactive) with a non-stoichiometric ratio of Ni–Cu–Zn in the starting chemical composition must be used [4]. It is known that the magnetic properties of spinel ferrite are strongly dependent on microstructure. Small amount of additives are often used for microstructure refinement. The rare earth oxides are becoming the promising additives for the improvement ferrite properties. Researches have been carried out about the influence of different rare earth atoms on the properties of Ni–Zn ferrite [5] and [6], Mn–Zn ferrite [7], Mg–Cu ferrite [8], Cu–Zn ferrite [9] and [10], etc. The results of these researches show that different rear-earth atoms behave differently in spinel ferrite. In general, the permeability of ferrite (e.g. Ni–Zn) was reported to decrease with the substitution of R_2O_3 [5] and [6]. Whereas, Sattar et al. [9] reported an increase of about 60% relative permeability in Sm-doped Cu–Zn ferrite. Some literature reported the decrease in relative density of ferrites with rare earth addition [5]; on the other hand others reported its increase [6], [7] and [8]. It has been accepted that the rare-earth ions commonly reside at octahedral sites [11] and have limited solubility in the spinel lattice due to their large ionic radii. But the precise value of their solubility in the spinel lattice is not known.

In this background, the effect of La substitution on the properties of Ni–Cu–Zn ferrite has been investigated to provide an accurate understanding of the changes caused by the substitution. To date, no literature is available reporting the effect of rare earth atom on the properties of Ni–Cu–Zn ferrite. In this study, a significant improvement in relative permeability of the ferrite has been achieved with a small fraction of La substitution, which is very promising from the technological point of view. The effect of La^{3+} substitution for Fe^{3+} on the microstructure, relative density, permeability and Curie temperature of Ni–Cu–Zn ferrite has been described. A Rietveld structure refinement was carried out to see the origin of the enhanced magnetic properties with La substitution had a structural origin.

2. Experimental

The ferrite powders are synthesized through a nitrate–citrate auto-combustion method for achieving homogeneous mixing of the component on the atomic scale and better sinterability of synthesized powder [12]. Analytical grade nickel nitrate [$Ni(NO_3)_2{\cdot}6H_2O$], zinc nitrate [$Zn(NO_3)_2{\cdot}6H_2O$], copper nitrate [$Cu(NO_3)_2{\cdot}3H_2O$], iron nitrate [$Fe(NO_3)_3{\cdot}9H_2O$], citric acid [$C_6H_8O_7{\cdot}H_2O$] and lanthanum nitrate [$La(NO_3)_3$] were used to prepare $(Ni_{0.25}Cu_{0.20}Zn_{0.55})La_xFe_{2-x}O_4$ ferrite with $x = 0.0$, 0.025, 0.050 and 0.075 compositions. Metal nitrates and citric acid were dissolved in deionized water. The molarities of different nitrate solutions were determined by using standard EDTA titration. Nitrates and citric acid solutions were mixed in 1:1 molar ratio of nitrates to citric acid. The pH of the solution was adjusted to 7 using ammonia solution. The solution was first heated at 80 °C to transform it into a gel and then ignited in a self-

propagating combustion manner to form a fluffy loose powder. The as-burnt precursor powder was then calcined at 700 °C for 2 h. The calcined powder was granulated using PVA as a binder and was uniaxially pressed at a pressure of 5 t/cm^2 to form toroidal and pellet specimens. The specimens were sintered at 900 °C for 4 h in air. The ferrites were characterized by X-ray diffraction (PW-1830, Philips, Netherlands) with Cu Kα radiation. For Rietveld refinement, slow step scanning data was taken with step size 0.02, 10 s/step, in the 2θ range 15–90°. The bulk density and porosity was measured using the Archimedes principle. An impendence analyzer (Hewlett Packard, Model 4192A, USA) was used to measure inductance on the toroidal samples, wound with low capacitive six turns enameled copper wire. Microstructures and chemical composition details were analyzed by using Scanning Electron Microscope (LEO 430i Stereoscan, UK) and an energy-dispersive X-ray analyzer (EDX).

3. Results and discussion

3.1. X-ray analysis

The La-doped Ni–Cu–Zn ferrite, was extensively characterized by XRD. The phase analysis showed that the as-burnt ferrite powders are crystalline in nature and contain cubic spinel ferrite phases as reported previously [12]. As-burnt powders were then calcined at 700 °C for 2 h to form homogeneous ferrite powders with proper distribution of cations. To identify the possible formation of a second phase ($LaFeO_3$) in substituted ferrite, the slow step scan XRD analysis was conducted on the samples after different stages of processing. Fig. 1 shows the step scan XRD pattern of as-burnt, calcined and sintered ferrite for $x = 0.025$ (Fig. 1(A)) and $x = 0.075$ (Fig. 1(B)) compositions, respectively. $LaFeO_3$ was not detected in all raw powders and in calcined powder of $x = 0.025$ composition. However, the phase was detected in calcined powder of $x = 0.075$ composition and in all sintered pellets. The absence of $LaFeO_3$ in as-burnt powders may be due to the formation of amorphous/non-crystalline product of the same by very rapid rate of combustion reaction. Upon increased heat treatment (e.g. calcinations and sintering), the crystallinity of the phase increases both in calcined and sintered products. That $LaFeO_3$ peaks were not found in the calcined powder of $x = 0.025$ composition, may be due to the presence only a very little amount of crystalline $LaFeO_3$.

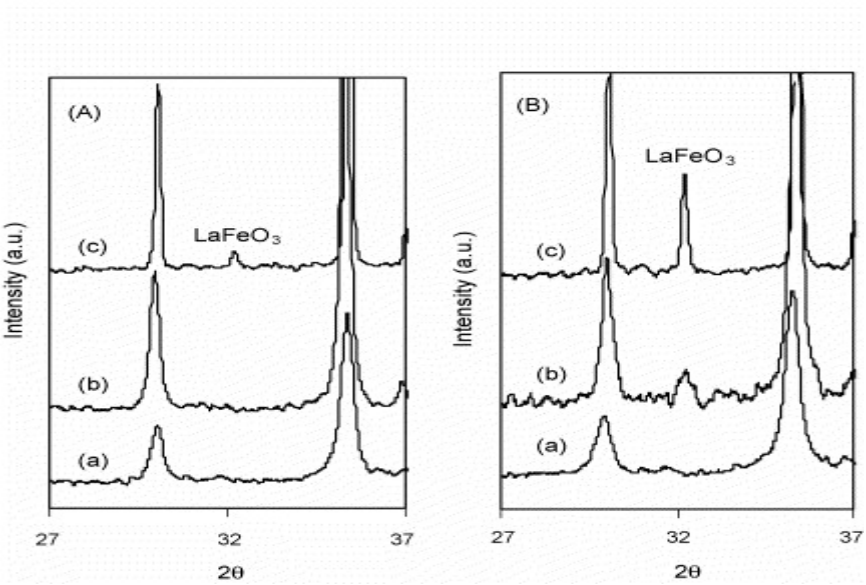

Fig. 1. XRD patterns of $(Ni_{0.25}Cu_{0.20}Zn_{0.55})La_xFe_{2-x}O_4$ ferrites with (A) $x = 0.025$, (B) $x = 0.075$ and in each (a) as-burnt powder (b) calcined powder and (c) sintered pellets.

Fig. 2 shows the step scan XRD patterns of different sintered ferrite pellets along with that of the undoped calcined ferrite powder. All the compositions show the presence of cubic spinel as a major phase. La-doped samples (Fig. 2(c)–(e)) show the presence of $LaFeO_3$ phase along with the major ferrite one. The intensity of $LaFeO_3$ increases with the increase in La concentration. This apparently indicates that the La does not form a solid solution with spinel ferrite or La^{3+} have limited solid solubility. One more interesting observation by slow step scanning is that a small unidentified phase peak appears in the sintered undoped ferrite. However, the above peak was not found in the calcined powder of the same (Fig. 2(a)), as well as in the La-doped sintered pellets. The identification of that very small peak was difficult. Many investigators reported that Ni–Cu–Zn ferrite dissociates during sintering to precipitate Cu metal or its oxide [1] and [4]. On this line, the peak was tried to match with Cu and/or Cu–O containing compounds. The matching suggests that the peak may be corresponding to some Cu–O containing phase with composition between Cu_2O–Cu_4O_3. The presence of Cu–O containing phase may be due to the surface oxidation of the precipitated Cu metal during sintering in air. The absence of that peak in the calcined powder may be due to the lower temperature heat treatment (700 °C/2 h) of loose powder compared to high temperature (900 °C/4 h) sintering of compact pellet. It is interesting to note that the peak was absent in La substituted samples. This may be due to the solubility of Cu in $LaFeO_3$ produced in the doped ceramics.

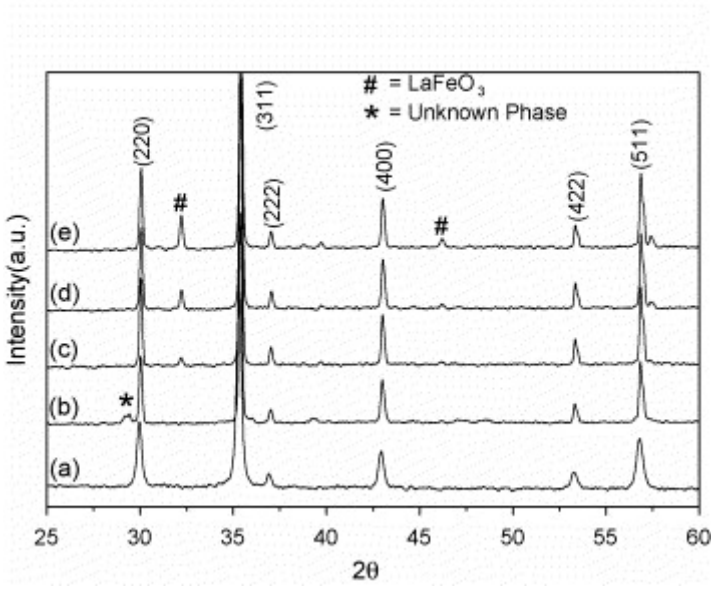

Fig. 2. XRD patterns of $(Ni_{0.25}Cu_{0.20}Zn_{0.55})La_xFe_{2-x}O_4$ ferrites (a) undoped calcined powder and sintered pellets of (b) $x = 0.00$, (c) $x = 0.025$, (d) $x = 0.050$, and (e) $x = 0.075$.

The Rietveld structure refinement was carried out to determine the (a) amount of $LaFeO_3$ formed (b) accurate lattice parameter (c) La-occupancy in the spinel lattice (d) residual stress/strain in sintered ferrite, etc. The program MAUDWEB version 2.031 was used for the Rietveld refinement [13]. Fig. 3 shows the observed, calculated profiles and their differences after the refinement for two representative phases (spinel and $LaFeO_3$) of composition $x = 0.075$. XRD data for the refinement was obtained from sintered pellets to estimate actual stress/strain present in solid ferrite body. The refinements were very good yielding a low *R*-factor for all the compositions. Some important refined parameters are shown in Table 1. The cell edges, a_0, were in the same range for different compositions. It has been reported that lattice constant increased by the incorporation of La in Mg–Cu ferrite [8]. However, no significant increase in a_0 was observed in the present experiment. There was a slight decrease in a_0 for $x = 0.025$ and slight increase for $x = 0.075$ compositions, respectively. Crystallite size and micro-strain were refined using Popa Line Broadening and isotropic size/strain model. Crystallite sizes were in the range 123–186 nm. It is interesting to note that the crystallite size (coherently scatter zone) of the ferrite (123 nm for undoped) was increased by about 50% (185 nm for $x = 0.025$ composition) upon a small fraction of La substitution. There were no significant changes in rms microstrain in different pellets samples. The macrostresses present in the pellets were calculated using advanced "Triaxial Stress Isotropic E" model available in the MAUD program. Significant differences in macrostresses were found in La-doped pellets compared to undoped one. The macrostress was more compressive (negative value) on La-doped pellets (except for $x = 0.075$). That may be due to the compressive pressure exerted by the $LaFeO_3$ present at the grain boundaries. A slightly lower a_0 value found in $x = 0.025$ may be due to this compressive stress. A tensile macrostress (positive value) was found in $x = 0.075$ compositions though it contains highest amount of $LaFeO_3$ phase.

The reason for this is not known. A slight increase in lattice parameter of this composition may be due to tensile stress.

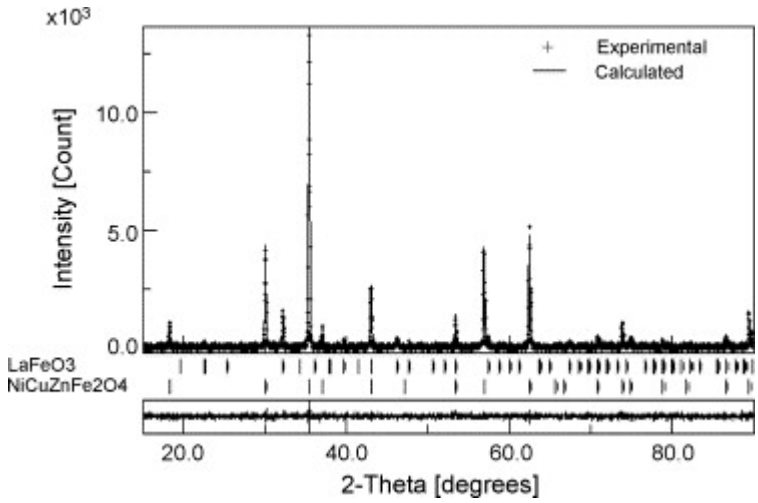

Fig. 3. Comparison between experimental (+) and calculated (−) X-ray diffraction pattern of $(Ni_{0.25}Cu_{0.20}Zn_{0.55})La_{0.075}Fe_{1.925}O_4$ ferrite fitted for spinel and $LaFeO_3$ phases. Difference between observed and calculated pattern is given in the bar.

Table 1.

Refined cell parameter, crystallite size, micro-strain, macrostress, %$LaFeO_3$ phase content, agreement factors (*R*-factors) and goodness of fit (GOF) obtained from Rietveld fits for $(Ni_{0.25}Cu_{0.20}Zn_{0.55})La_xFe_{2-x}O_4$ ferrites with $x = 0.00$, 0.025, 0.050 and 0.075

Parameters	**Composition**			
	***x* = 0.0**	***x* = 0.025**	***x* = 0.050**	***x* = 0.075**
a_0 (Å)	8.4096(3)	8.4004(8)	8.4053(7)	8.4112(4)
Crystallite size (nm)	123	186	152	158
rms microstrain	3.8×10^{-4}	3.17×10^{-4}	3.3×10^{-4}	3.2×10^{-4}
Macrostress (11)	-3.7×10^{-9}	−0.31	−0.30	0.033
%$LaFeO_3$	0	1.34	3.4	5.4
R_{wp} (%)	2.04	1.76	1.82	1.81

Parameters	Composition			
	$x = 0.0$	$x = 0.025$	$x = 0.050$	$x = 0.075$
R_p (%)	1.58	1.39	1.43	1.44
GOF	1.15	1.09	1.10	1.08

Regarding $LaFeO_3$ phase formation, if we consider La forms solely $LaFeO_3$ without entering into the spinel lattice, then about 2.4, 5.0 and 7.4 wt.% $LaFeO_3$ should be formed in the compositions with $x = 0.025$, 0.050 and 0.075, respectively. However, the quantitative estimation (Table 1) shows a slight lower (1–2 wt.%) amount of $LaFeO_3$ in them. This may be due to the incorporation of remaining La into the spinel lattice and/or presence of small amorphous phase of it. During structure refinement, it was found that the occupancy of octahedral site tends to increase above the permitted 16 atoms/unit cell for La-doped compositions. This may be due to the requirement of excess scattering factor at the sites. Since, Fe, Ni, Cu, etc. have equivalent scattering factors, there is some possibility of presence of La having almost double scattering factor than others. Accordingly, octahedral occupancy was refined allowing La to occupy the site. However, the refinement yields only about 0.05–0.08 La/unit cell occupancy. This is equivalent to about 1–2 wt.% $LaFeO_3$, which was not found in quantitative estimation. The observation indicates that La has very low solubility in spinel lattice due to its bigger ionic radii. Lattice parameters values also suggest the same as there were very small changes in it.

3.2. Microstructure and densification

Fig. 4 shows the microstructure of sintered pellets. The undoped sample (Fig. 4A) shows the presence of a monophasic spinel phase. Whereas, the La-doped materials show (Fig. 4B–D) a bi-phasic microstructure consisting of a bigger matrix of ferrite grains and a smaller $LaFeO_3$ secondary phase at the grain junctions/boundaries. The EDS spectra obtained from the center of grain boundary $LaFeO_3$ phase indicated the presence of mainly La, Fe and oxygen along with small amount of Cu, Ni and Zn. The grain size of matrix ferrite phase as well as the $LaFeO_3$ phase increased with increasing the La^{3+} substitutions. The average grain sizes of the ferrite matrix phase in different samples are shown in Table 2. The EDS spectra obtained from the center of La-doped Ni–Cu–Zn ferrite grains indicated the presence of small concentration La inside grains (Fig. 5).

Fig. 4. SEM photographs of sintered $(Ni_{0.25}Cu_{0.20}Zn_{0.55})La_xFe_{2-x}O_4$ ferrites with (A) $x = 0.00$, (B) $x = 0.025$, (C) $x = 0.050$, and (D) $x = 0.075$.

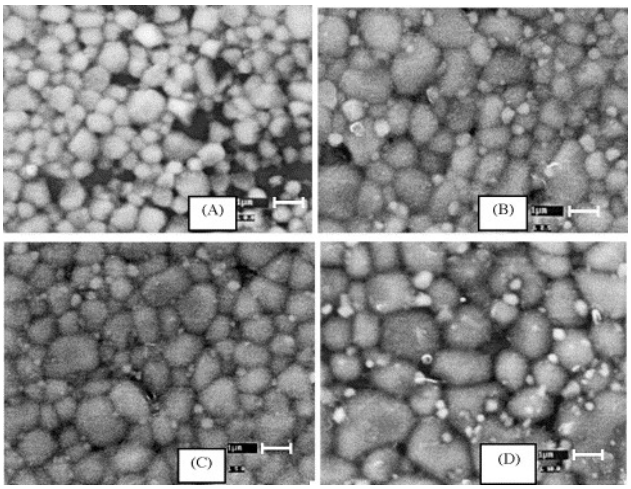

Table 2.

Bulk density, apparent porosity, grain size, permeability and Curie temperature of sintered $(Ni_{0.25}Cu_{0.20}Zn_{0.55})La_xFe_{2-x}O_4$ ferrites with different La(x) content

x **(La-content)**	**Bulk density (g/cm^3)**	**Apparent porosity (%)**	**Grain size (μm)**	**Permeability (μm)**	**Curie temperature (°C)**
0.00	4.61	11.6	0.65	202	185
0.025	4.85	2.3	0.88	424	190
0.050	4.98	1.3	0.92	249	185
0.075	5.04	1.2	1.17	198	187

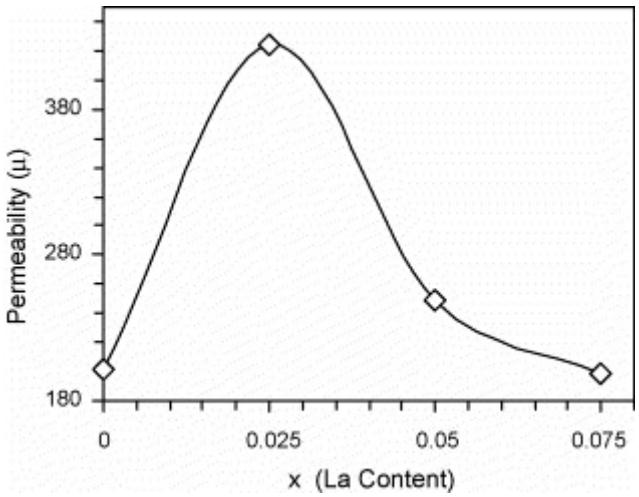

Fig. 5. Initial permeability as a function of La(x) substitution in $(Ni_{0.25}Cu_{0.20}Zn_{0.55})La_xFe_{2-x}O_4$ ferrites.

Table 2 shows the bulk density, apparent porosity of different samples along with their grain size, initial permeability and Curie temperature. The bulk density and grain size increases with the increase in La content, indicating the improved densification and grain growth upon La addition. Simultaneously, the apparent porosity decreases with La addition. It has been reported that the bulk density of Ni–Zn ferrite decreased upon La addition [5], whereas, that of Mg–Cu ferrite increased [8]. The increased densification in this case is due to the presence of excess Cu, Ni and Zn in the system. The excess Cu, Ni and Zn arises due to the La substitution for Fe in the ferrite, i.e. the La-substituted compositions are Fe deficient with respect to undoped composition. As we have seen, La forms $LaFeO_3$ in the system; it further takes some more Fe from the composition. The neat result is that the composition has non-stoichiometric excess Ni–Cu–Zn. This non-stoichiometry increases with the increase in %La substitution. It is known that, the non-stoichiometric excess Ni–Cu–Zn is used for low temperature liquid phase sintering of the ferrite. For this reason the densification increases with La substitution.

3.3. Magnetic properties

The change in initial permeability of Ni–Cu–Zn ferrite with La substitution is shown in Fig. 4 (the values are shown in Table 2). It is interesting to note that the initial permeability significantly increases at $x = 0.025$ of La substitution. The similar increase in permeability of Cu–Zn ferrite with Sm substitution for Fe was also reported by Sattar et al. [9]. La^{3+} has no unpaired electrons and it behaves as paramagnetic. The substitution of ferromagnetic Fe^{3+} ($5\mu_B$) by paramagnetic La^{3+} in the spinel is not useful for increasing magnetization. It has been suggested that the substitution of Sm^{3+} ion moves Cu^{2+} and Zn^{2+} ion from 'B' to 'A' site causing 'A'-sublattice dilution and increased magnetization in Cu–Zn ferrite [10]. However, in the present case La^{3+} incorporation into the lattice was very small ($\sim$0.1 atom/unit cell) and hence the increased permeability is not due to its incorporation. The increased permeability at $x = 0.025$ compared to undoped one may be due to the following reasons: (a) increased grain size, a specially increased crystallite size; (b) increased density as well as decreased porosity; (c) decreased magnetocrystalline anisotropy; (d) change in stress; (e) absence of the Cu-containing non-magnetic precipitated compound due to the solid-solution formation of Cu in $LaFeO_3$, etc.

It is well established that the permeability increases with the increase in density, grain size and with the decrease in porosity in polycrystalline ferrite. The initial permeability of ferrite is usually expressed [4] as $\mu_i = M_s^2/(aK + b\lambda\sigma)$, where μ_i is the initial permeability, M_s the saturation magnetization, K the crystal magnetic anisotropy, λ the magnetostriction constant, σ the inner stress and a,b are constants. Thus, the initial permeability is strongly influenced by anisotropy, magnetostriction and stress. The magnetic anisotropy field in ferrites results mainly from Fe^{2+} ions [14]. The La-substituted compositions are deficient in Fe and hence Fe^{2+} ions are expected to be at minimum. The magnetic anisotropy is also expected to decrease. The compressive

macrostress (Table 1) in $x = 0.025$ composition is higher than undoped. The stress in the undoped sample may be considered as zero (as in the order of 10^{-8}). A compressive stress can increase the initial permeability of ferrite with negative magnetostriction [15]. So the increased permeability in $x = 0.025$ composition is, partly due to the higher compressive stress prevailing in the sample. However, the permeability decreased with higher La ($>x = 0.025$) substitution. This may be due to the decrease in high permeability Ni–Cu–Zn ferrite at the expanse of $LaFeO_3$ phase. One more reason may be the change in macrostress. As stated earlier, a tensile macrostress was found in $x = 0.075$ samples and the decreased permeability is due to that tensile stress [15]. Finally, the change in Curie temperature of the ferrite with La substitution was also evaluated. No significant change in Curie temperature (Table 2) was found with La substitution. This again indicates that La has very low solubility in spinel ferrite.

4. Conclusions

It may be concluded that the substitution of La for Fe in Ni–Cu–Zn ferrite mainly produces secondary phase $LaFeO_3$. An amorphous $LaFeO_3$ phase is formed during nitrate–citrate auto-combustion synthesis of the substituted ferrite and the crystallinity of it increases upon successive heat treatment. Relative density and grain size of the ferrite increases with the increase in La substitution mainly due to the increase in non-stoichiometric Cu content. A Cu-containing oxide phase was found to precipitate during sintering of undoped Ni–Cu–Zn ferrite. However, that Cu-containing phase was not found in La-substituted ferrite due to the solid solution formation of Cu within $LaFeO_3$. A significant increase in initial permeability of the ferrite was found at small fraction of La ($x = 0.025$) substitution. The increased permeability is due to the combined effect of increased grain size, specially increased crystallite size, increased densification (decreased porosity), decreased anisotropy and compressive macrostress. The La solubility in the Ni–Cu–Zn ferrite lattice was found very low ($\sim$0.1 atom/unit cell).

Acknowledgement

J. Bera wishes to thank the Department of Science & Technology, Government of India, New Delhi, for providing financial support through project grant (Grant no. SR/S3/ME/04/2002-SERC-Engg).

References

[1] K.O. Low and F.R. Sale, *J. Magn. Magn. Mater.* **246** (2002), pp. 30–35. Abstract | **Full Text + Links** | PDF (125 K) | Abstract + References in Scopus | Cited By in Scopus

[2] D. Stoppels, *J. Magn. Magn. Mater.* **160** (1996), p. 323. Abstract | **Full Text + Links** | PDF (485 K) | Abstract + References in Scopus | Cited By in Scopus

[3] H.I. Hsiang, W.C. Liao, Y.J. Wang and Y.F. Cheng, *J. Eur. Ceram. Soc.* **24** (2004), pp. 2015–2021. SummaryPlus | **Full Text + Links** | PDF (504 K) | Abstract + References in Scopus | Cited By in Scopus

[4] M. Fujimoto, *J. Am. Ceram. Soc.* **77** (1994) (11), pp. 2873–2878. Abstract-INSPEC | Abstract-Compendex | **Full Text** via CrossRef | Abstract + References in Scopus | Cited By in Scopus

[5] J. Sun, J. Li and G. Sun, *J. Magn. Magn. Mater.* **250** (2002), pp. 20–24. Abstract | **Full Text + Links** | PDF (145 K) | Abstract + References in Scopus | Cited By in Scopus

[6] A.C.F.M. Costa, M.R. Morelli and R.H.G.A. Kiminami, *J. Mater. Sci.* **39** (2004), pp. 1773–1776.

[7] M.A. Ahmed, N. Okasha, M.M. El-Sayed, Ceram. Int., in press.

[8] E. Rezlescu, N. Rezlescu and P.D. Popa, *J. Magn. Magn. Mater.* **290/291** (2005), pp. 1001–1004. Abstract | **Full Text + Links** | PDF (204 K) | Abstract + References in Scopus | Cited By in Scopus

[9] A.A. Sattar *et al.*, *Phys. Stat. Sol.* **171** (1999), p. 563. Abstract-INSPEC | Abstract-Compendex | **Full Text** via CrossRef | Abstract + References in Scopus | Cited By in Scopus

[10] M.H. Mahmoud and A.A. Sattar, *J. Magn. Magn. Mater.* **277** (2004), pp. 101–105. Abstract | **Full Text + Links** | PDF (235 K) | Abstract + References in Scopus | Cited By in Scopus

[11] A.A. Sattar and K.M. El-Shokrofy, *J. Phys. IV* **C1** (1997), p. 245. Abstract-Compendex | Abstract-INSPEC | Abstract + References in Scopus | Cited By in Scopus

[12] P.K. Roy and J. Bera, *J. Magn. Magn. Mater.* **298** (2006), pp. 38–42. Abstract | **Full Text + Links** | PDF (210 K) | Abstract + References in Scopus | Cited By in Scopus

[13] http://www.ing.unitn.it/~maud

[14] E.W. Gorter, *Philips Res. Rep.* **9** (1954), p. 295.

[15] J. Smit and H.P.J. Wijn, Ferrites, John Wiley & Sons, New York (1959) 265.